

# Many-body effects in twisted bilayer graphene at low twist angles

A.O. Sboychakov,<sup>1,2</sup> A.V. Rozhkov,<sup>1,2,3,4</sup> A.L. Rakhmanov,<sup>1,2,3,5</sup> and Franco Nori<sup>1,6</sup>

<sup>1</sup>*Theoretical Quantum Physics Laboratory, RIKEN, Wako-shi, Saitama, 351-0198, Japan*

<sup>2</sup>*Institute for Theoretical and Applied Electrodynamics,  
Russian Academy of Sciences, Moscow, 125412 Russia*

<sup>3</sup>*Moscow Institute for Physics and Technology (State University), Dolgoprudnyi, 141700 Russia*

<sup>4</sup>*Skolkovo Institute of Science and Technology, Skolkovo Innovation Center 3, Moscow 143026, Russia*

<sup>5</sup>*Dukhov Research Institute of Automatics, Moscow, 127055 Russia*

<sup>6</sup>*Department of Physics, University of Michigan, Ann Arbor, MI 48109-1040, USA*

(Dated: May 15, 2019)

We study the mean-field zero-temperature many-body properties of twisted bilayer graphene with a twist angle equal to the so-called ‘first magic angle’. Its low-energy spectrum consists of four weakly-dispersing partially degenerate single-electron bands. The band flatness makes electrons susceptible to the effects of the interactions. We consider two excitonic order parameters with spin-density-wave-like structure, and demonstrate that they lift the band degeneracy. One of these order parameters generates a spectral gap at zero doping, while the other opens the gap when the doping  $n$  equals to two electrons per supercell. We find that the order parameters depend non-trivially on the doping level. The order parameters variation versus doping allows us to reproduce qualitatively the behavior of the conductivity, which was recently observed experimentally [Cao et al., *Nature* **556**, 80 (2018)].

PACS numbers: 73.22.Pr, 73.21.Ac

*Introduction*— The search for broken-symmetry phases in graphene bilayer systems remains an active research area [1]. Theorists have studied a variety of possibilities, such as antiferromagnetism [2–10] superconductivity [11–14], excitons [3, 15–17], as well as more exotic states [5, 18] Unfortunately, experimentally, the broken symmetry phases are rare celebrities in graphene systems, except, perhaps, AB bilayer graphene, for which numerous experiments [19–24] provide evidence of the low temperature non-superconducting order. It appears, however, that the situation in this field has changed: in recent experiments [25, 26] both superconductivity and many-body insulating states were detected in doped samples of twisted bilayer graphene (TBLG) whose twist angle  $\theta$  equals to the so-called ‘first magic angle’  $\theta_c$ . The dependence of the conductivity  $\sigma$ , measured as a function of doping  $n$ , showed several pronounced minima: at  $n = 0$  (charge neutrality point), at  $n = \pm n_s/2$ , and at  $n = n_s$  (doping level  $n = n_s$  corresponds to one electron per spin projection per layer per supercell, or, equivalently, four electrons per supercell). The authors argued that the minima of  $\sigma(n)$  at  $n = \pm n_s/2$  are of many-body nature. The purpose of this paper is to offer a theoretical discussion of these findings.

Our argument relies on the peculiar structure of the low-energy spectrum of TBLG at small twist angles  $\theta$ . For the TBLG it is known that the Dirac cones [27–31] at  $\theta > \theta_c$  are replaced by four low-energy bands with almost no dispersion when  $\theta \leq \theta_c$ . The minima of conductivity at  $n = \pm n_s$  are associated with the single-particle density of states (DOS) of these bands. Explanations of other conductivity minima require a many-body formalism. The emergent bands are partially degenerate. Be-

cause of their flatness and degeneracy, interaction effects are important. We use a mean field approach to account for interactions. Introducing excitonic spin-density wave (SDW) order parameter, we show that the degeneracy is partially lifted: the bands (partially) split up in energy space. Therefore, at  $n = 0$  the spectrum develops a gap at the chemical potential, and the conductivity minimum emerges, in agreement with the experiment [25]. To explain the behavior of  $\sigma(n)$  at  $|n| = n_s/2$ , we need to introduce yet another, inter-layer SDW order parameter which lifts the remaining degeneracy, generating the desired gap. Our formalism captures qualitatively the dependence of  $\sigma$  versus doping reported in Ref. 25.

*Geometry of twisted bilayer graphene*— Let us first review the basic geometric facts of TBLG to briefly introduce the notation. (For a comprehensive account, one may consult Refs. [1, 30, 32].) A graphene monolayer has a hexagonal crystal structure consisting of two triangular sublattices  $A$  and  $B$ . The coordinates of atoms in layer 1 are  $\mathbf{r}_n^{1A} = \mathbf{r}_n^1 \equiv n\mathbf{a}_1 + m\mathbf{a}_2$  and  $\mathbf{r}_n^{1B} = \mathbf{r}_n^1 + \boldsymbol{\delta}$ , where  $\mathbf{n} = (n, m)$  is an integer-valued vector,  $\mathbf{a}_{1,2} = a(\sqrt{3}, \mp 1)/2$  are the primitive vectors ( $a = 2.46 \text{ \AA}$ ), and  $\boldsymbol{\delta} = a(1/\sqrt{3}, 0)$ . Atoms in layer 2 are located at  $\mathbf{r}_n^{2B} = \mathbf{r}_n^2 \equiv d\mathbf{e}_z + n\mathbf{a}'_1 + m\mathbf{a}'_2$  and  $\mathbf{r}_n^{2A} = \mathbf{r}_n^2 - \boldsymbol{\delta}'$ , where  $(\mathbf{a}'_{1,2}, \boldsymbol{\delta}')$  are the vectors  $(\mathbf{a}_{1,2}, \boldsymbol{\delta})$  rotated by an angle  $\theta$ , and  $\mathbf{e}_z$  denotes the unit vector along the  $z$ -axis. The interlayer distance is  $d = 3.35 \text{ \AA}$ . The limiting case  $\theta = 0$  corresponds to the AB stacking. The superstructure exists if  $\cos\theta = (3m_0^2 + 3m_0r + r^2/2)/(3m_0^2 + 3m_0r + r^2)$ , where  $m_0$  and  $r$  are co-prime positive integers. The number of graphene unit cells inside a supercell is  $N_{sc} = (3m_0^2 + 3m_0r + r^2)/g$  per layer, where  $g = 1$  if  $r \neq 3n$ , or  $g = 3$  otherwise. The reciprocal lattice primitive vectors for the layer 1

(layer 2) are denoted by  $\mathbf{b}_{1,2}$  ( $\mathbf{b}'_{1,2}$ ). For layer 1 one has  $\mathbf{b}_{1,2} = 2\pi(1/\sqrt{3}, \mp 1)/a$ , while  $\mathbf{b}'_{1,2}$  are connected to  $\mathbf{b}_{1,2}$  by rotating an angle  $\theta$ . Using the notation  $\mathcal{G}_{1,2}$  for the primitive reciprocal vectors for the superlattice, the following identities may be proven:  $\mathbf{b}'_1 = \mathbf{b}_1 + r(\mathcal{G}_1 + \mathcal{G}_2)$  and  $\mathbf{b}'_2 = \mathbf{b}_2 - r\mathcal{G}_1$  if  $r \neq 3n$ , or  $\mathbf{b}'_1 = \mathbf{b}_1 + r(\mathcal{G}_1 + 2\mathcal{G}_2)/3$  and  $\mathbf{b}'_2 = \mathbf{b}_2 - r(2\mathcal{G}_1 + \mathcal{G}_2)/3$ , otherwise. The Brillouin zone of the superlattice is hexagonal-shaped. It can be obtained by  $N_{sc}$ -times folding of the Brillouin zone of the layer 1 or 2. Two non-equivalent corners of the reduced Brillouin zone,  $\mathbf{K}_1$  and  $\mathbf{K}_2$ , can be expressed via vectors  $\mathcal{G}_{1,2}$  as  $\mathbf{K}_1 = (\mathcal{G}_1 + 2\mathcal{G}_2)/3$  and  $\mathbf{K}_2 = (2\mathcal{G}_1 + \mathcal{G}_2)/3$ .

*Model Hamiltonian.*— We investigate the tight-binding model for  $p_z$  electrons in the TBLG at small doping  $n$ . The Hamiltonian is  $\hat{H} = \hat{H}_0 + \hat{H}_{int}$ , where  $\hat{H}_0$  is a single-electron Hamiltonian, and  $\hat{H}_{int}$  describes the electron-electron interaction. The single-electron Hamiltonian is

$$\hat{H}_0 = \sum_{\substack{injm \\ ss'\sigma}} t(\mathbf{r}_n^{is}; \mathbf{r}_m^{js'}) \hat{d}_{nis\sigma}^\dagger \hat{d}_{mjs'\sigma}, \quad (1)$$

where  $\hat{d}_{nis\sigma}^\dagger$  ( $\hat{d}_{nis\sigma}$ ) are the creation (annihilation) operators of the electron with spin  $\sigma$  at the unit cell  $\mathbf{n}$  in the layer  $i$  ( $= 1, 2$ ) in the sublattice  $s$  ( $= A, B$ ). For intralayer hopping, only the nearest-neighbor term is included. Its amplitude is  $-t$ , where  $t = 2.57$  eV. The interlayer hopping is parameterized as described in Refs. [31, 33], with the largest interlayer hopping amplitude being equal to  $t_0 = 0.4$  eV. Switching to the momentum representation, one can introduce new single-particle operators  $\hat{d}_{\mathbf{p}\mathbf{G}is\sigma} = \mathcal{N}^{-1/2} \sum_{\mathbf{n}} e^{-i(\mathbf{p}+\mathbf{G})\mathbf{r}_n} \hat{d}_{nis\sigma}$ . Here  $\mathcal{N}$  is the number of graphene unit cells in the sample in one layer, the momentum  $\mathbf{p}$  lies in the first Brillouin zone of the superlattice, while  $\mathbf{G} = m_1\mathcal{G}_1 + m_2\mathcal{G}_2$  is the reciprocal vector of the superlattice lying in the first Brillouin zone of the  $i$ th layer. The number of such vectors  $\mathbf{G}$  is equal to  $N_{sc}$  for each graphene layer. Thus,  $\hat{H}_0$  becomes

$$\hat{H}_0 = \sum_{\mathbf{p}\mathbf{G}_{1,2}} \sum_{ijss'\sigma} \tilde{t}_{ij}^{ss'}(\mathbf{p}+\mathbf{G}_1; \mathbf{G}_1-\mathbf{G}_2) \hat{d}_{\mathbf{p}\mathbf{G}_1is\sigma}^\dagger \hat{d}_{\mathbf{p}\mathbf{G}_2js'\sigma}, \quad (2)$$

where the hopping amplitudes in momentum space are

$$\tilde{t}_{ij}^{ss'}(\mathbf{k}; \mathbf{G}) = \frac{1}{N_{sc}} \sum_{\mathbf{nm}}' e^{-i\mathbf{k}(\mathbf{r}_n^i - \mathbf{r}_m^j)} e^{-i\mathbf{G}\mathbf{r}_m^j} t(\mathbf{r}_n^{is}; \mathbf{r}_m^{js'}). \quad (3)$$

The summation with prime  $\sum_{\mathbf{nm}}'$  denotes that  $\mathbf{m}$  runs over sites inside the zeroth supercell, while  $\mathbf{n}$  runs over all sites in the sample.

The Hamiltonian (2) can be used to find numerically the single-electron spectrum  $E_{\mathbf{p}}^{(S)}$  and eigenvectors  $\Phi_{\mathbf{p}\mathbf{G}is}^{(S)}$ , where  $S = 1, 2, \dots, 4N_{sc}$  labels  $4N_{sc}$  single-electron bands. The spectrum of (2) is well-studied. Its properties at small and large  $\theta$  differ qualitatively. When  $\theta > \theta_c$  (for the hopping parameters used here  $\theta_c \cong 1.89^\circ$ ), the low-energy spectrum is Dirac-like. If

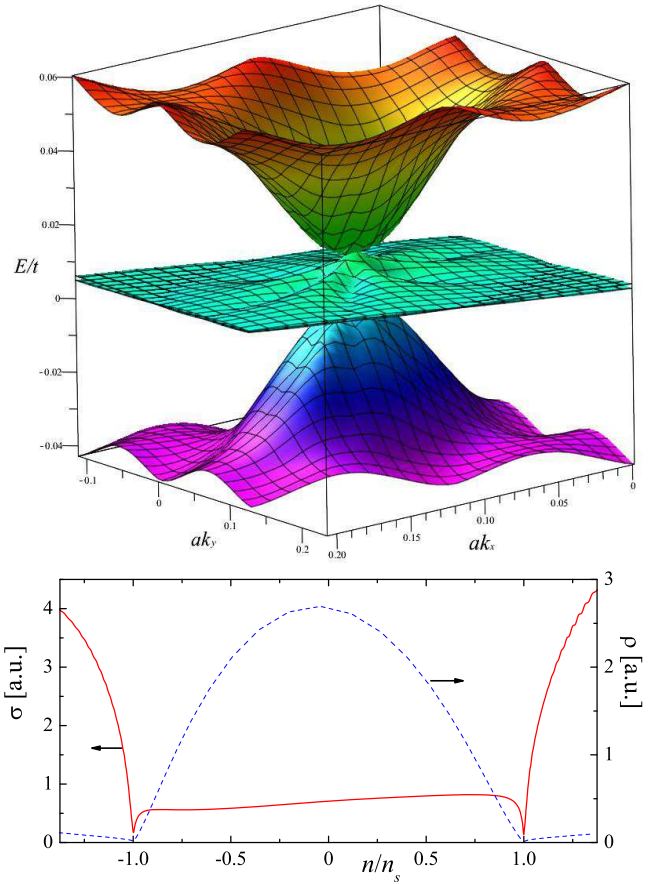


FIG. 1: (Top) Low-energy band structure inside the superlattice Brillouin zone calculated for the first magic angle  $\theta = \theta_c$ . Two nearly degenerate weakly-dispersing bands are clearly seen. (Bottom) The conductivity  $\sigma$  (solid curve) and density of states  $\rho$  (dashed curve) for the bands shown above are plotted versus the normalized charge concentration  $n/n_s$ .

$\theta \leq \theta_c$ , the Dirac cones are absent. Instead, there are four almost flat partially degenerate bands at low energy. For example, in Fig. 1 (top) the spectrum of this type is plotted for ‘the first magic angle’  $\theta = \theta_c$ . The electron and hole bands with pronounced dispersion are separated from each other by almost flat bands. This peculiar spectrum structure is the origin of the many-body physics discussed below.

The flat bands are not entirely dispersionless: we evaluate their width to be  $W \sim 20$  meV, which is consistent with other estimates [25, 26]. To compare our results against the experiment, it is convenient to calculate the DOS  $\rho(\varepsilon) = 2 \sum_S \int_{\mathbf{p}} \delta(E_{\mathbf{p}}^{(S)} - \varepsilon)$  as an (implicit) function of the doping level  $n(\varepsilon) = \int_0^\varepsilon \rho(\bar{\varepsilon}) d\bar{\varepsilon}$ , where  $\varepsilon = 0$  represents the charge neutrality point. The resultant plot is shown in Fig. 1 (bottom). Note that the low-energy spectrum is confined within the  $n = \pm n_s$  window, which is consistent with the presence of four weakly-dispersing bands, each of these bands accumulating up to one electron per spin projection per supercell (altogether, up to

eight electrons per supercell). In addition, Fig. 1 (bottom) presents the (direction-averaged) charge conductivity, calculated in the  $\tau$ -approximation, versus  $n$ :

$$\sigma = \frac{e^2}{4\pi^2} \sum_S \int d^2\mathbf{p} \left| \frac{\partial E_{\mathbf{p}}^{(S)}}{\partial \mathbf{p}} \right|^2 \delta(\mu - E_{\mathbf{p}}^{(S)}) \tau(\mathbf{p}), \quad (4)$$

where a momentum-independent transport scattering time  $\tau(\mathbf{k}) = \text{const.}$  is assumed. The conductivity shows a weak featureless dependence on  $n$  for  $|n| \lesssim n_s$ , see Fig. 1 (bottom).

*Interactions.*— Because of the weak dispersion, the low-energy electronic structure is affected strongly by the interaction. The many-body effects are studied below for the twist angle value  $\theta = \theta_c$ , in agreement with experimental conditions [25, 26]. As a starting point of our many-body analysis, we model  $\hat{H}_{\text{int}}$  using the Hubbard interaction

$$\hat{H}_{\text{int}} = \frac{U}{2} \sum_{\mathbf{n}i\sigma} \hat{d}_{\mathbf{n}i\sigma}^\dagger \hat{d}_{\mathbf{n}i\sigma} \hat{d}_{\mathbf{n}i\bar{\sigma}}^\dagger \hat{d}_{\mathbf{n}i\bar{\sigma}}, \quad (5)$$

$$U = 2t < U_c^{\text{MF}}. \quad (6)$$

Here  $U_c^{\text{MF}} \approx 2.23t$  is the critical strength for a single-layer graphene transition into a mean field antiferromagnetic state [34]. The choice (6) implies that the interaction in our model is strong, yet, not strong enough to cause a single-layer many-body instability, at least in the mean field framework. In other words, the presence of the second layer is a necessary prerequisite for a mean field transition. The notation  $\bar{\sigma}$  means ‘not  $\sigma$ ’.

*Two types of order parameters.*— To account for the interaction (5) at the mean field level, we must choose a suitable order parameter. Firstly, let us define [3, 7, 8, 10, 35] the on-site magnetization  $\eta_{\mathbf{m}i\sigma} = \langle \hat{d}_{\mathbf{m}i\sigma}^\dagger \hat{d}_{\mathbf{m}i\sigma} \rangle$ , where  $\langle \dots \rangle$  denotes the averaging with respect to the mean field ground state. We will assume that the anomalous average  $\eta_{\mathbf{m}i\sigma}$ , as a function of position  $\mathbf{m}$ , has the same period as the superlattice. That is, only the spin-rotational symmetry is broken, while the superlattice translation symmetry is preserved (the spin texture has the same periodicity as the superlattice). Using the  $\eta$ ’s we decouple  $H_{\text{int}}$ , to obtain the mean-field interaction

$$\hat{H}_{\text{int}}^{\text{MF}} = \sum_{\mathbf{n}i\sigma} \left[ -\Delta_{\mathbf{n}i\sigma} \hat{d}_{\mathbf{n}i\bar{\sigma}}^\dagger \hat{d}_{\mathbf{n}i\sigma} + \frac{|\Delta_{\mathbf{n}i\sigma}|^2}{U} \right], \quad (7)$$

where  $\Delta_{\mathbf{n}i\sigma} = U\eta_{\mathbf{n}i\sigma}$  is the order parameter. Finding the self-consistent value of  $\Delta_{\mathbf{n}i\sigma}$ , we can determine the low-energy band structure of our model, modified by the interaction. The outcome of such calculations at the charge neutrality point ( $n = 0$ ) is presented in Fig. 2 (top). Note that the degeneracy of the four bands is partially lifted. Two occupied bands are pushed to lower energies by the interaction effects, decreasing the system total energy. Two other bands are moved to

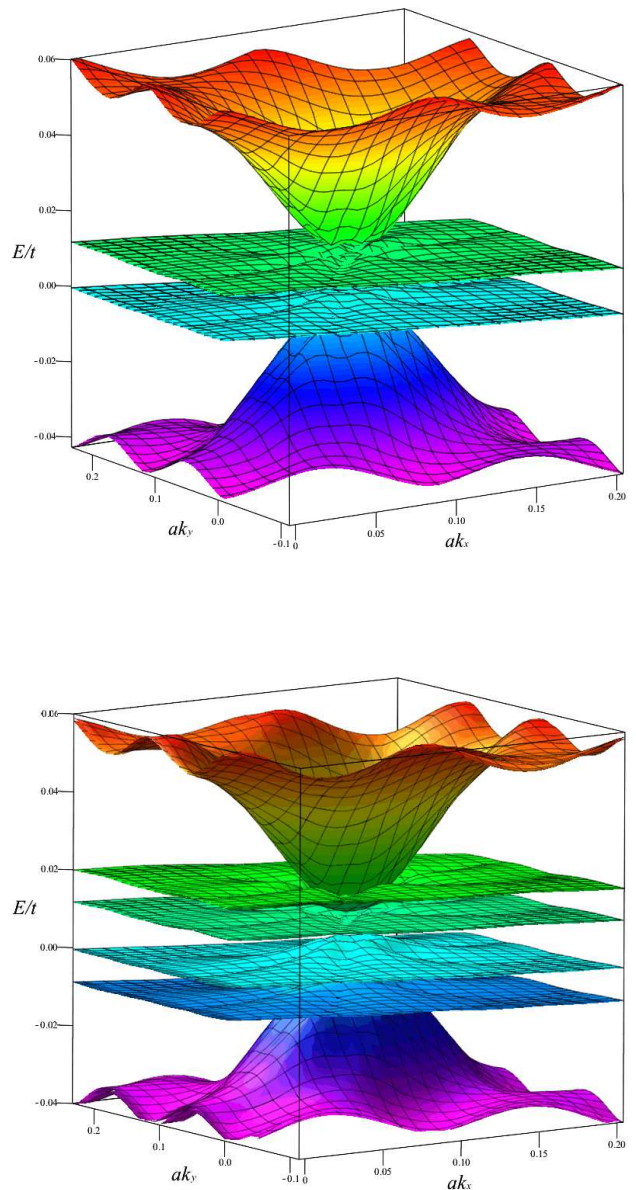


FIG. 2: (Top) Band structure near a corner of the superlattice Brillouin zone calculated for non-zero  $\Delta_{\mathbf{n}i\sigma}$ , found self-consistently. The degeneracy between low-energy bands are partially lifted. (Bottom) Non-zero  $\Delta_{\mathbf{n}i\sigma}^{\text{ex}}$  lifts the degeneracy completely. All four bands are now clearly visible.

higher energies; however, since they are empty, the system energy is unaffected by this change. The spectral gap is of the order of  $\Delta = 5.8 \times 10^{-3}t \cong 15 \text{ meV}$ .

Using Eq. (4), we can calculate the conductivity in this state, see Fig. 3 (a). The gap at  $\varepsilon = 0$  results in the pronounced conductivity drop at zero doping, consistent with data [25].

However, in the experiment [25] the TBLG sample demonstrated insulating behavior not only near  $n = 0$ , but near  $n \approx \pm n_s/2$  as well. The doping level  $n = \pm n_s/2$  corresponds to two electrons per supercell, or, equiv-

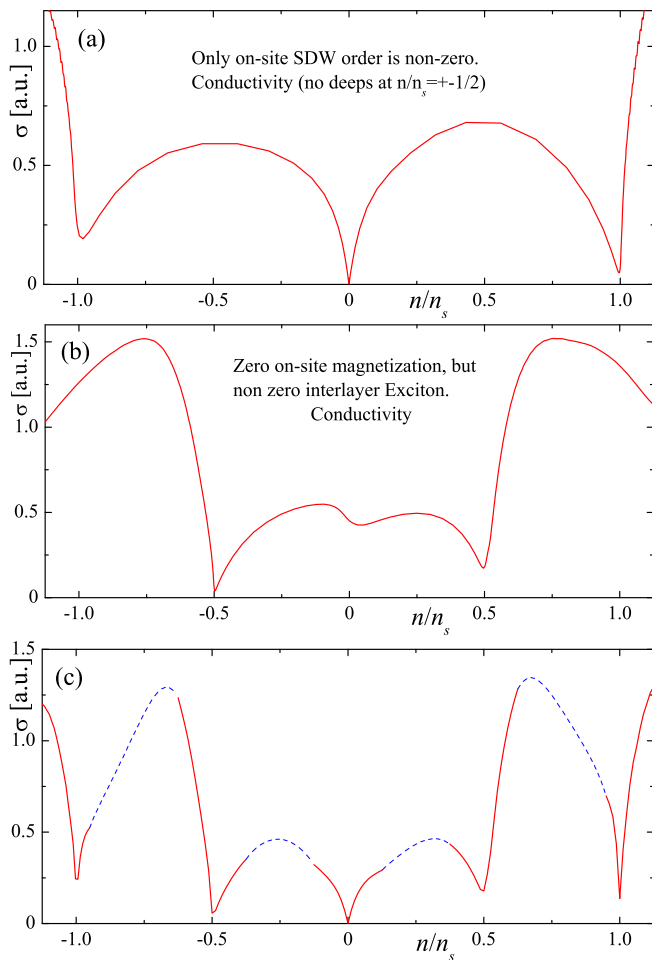


FIG. 3: (a) Conductivity at finite  $\Delta_{\mathbf{m}i\sigma}$ , but zero  $\Delta^{\text{ex}}$ . (b) Conductivity at zero  $\Delta_{\mathbf{m}i\sigma}$ , but finite  $\Delta^{\text{ex}}$ . (c) This plot for  $\sigma(n)$  accounts for variations of both order parameters with doping. Near charge neutrality,  $\sigma(n)$  is approximated by the curve calculated for finite  $\Delta_{\mathbf{m}i\sigma}$ , but  $\Delta^{\text{ex}} = 0$ . For  $n$  near  $|n|/n_s \approx 0.5$ , we use  $\Delta_{\mathbf{m}i\sigma} = 0$ ,  $\Delta^{\text{ex}} = 1.5 \times 10^{-3}t \cong 3.9$  meV to determine  $\sigma$ . For larger doping values,  $\Delta^{\text{ex}} = \Delta_{\mathbf{m}i\sigma} = 0$ . The blue (dashed) curves are interpolations between the three regimes.

alently, to complete filling (complete draining) of exactly one single-particle superlattice band. Theoretically, to have an insulating state at this doping, all added (drained) charge must completely fill (completely drain) a single electron band. Instead, the spectrum of Fig. 2 (top) implies that this charge will be shared between two bands: for example, if we add electrons, both bands at  $E \approx 0.01t$  absorb extra carriers, and in the range  $0 < n < n_s$  each band of this pair becomes fractionally filled. As a result, a multi-component metallic Fermi surface, resembling the one discussed in Ref. [31], is formed. The situation with hole doping is similar, with only one minor modification: for  $0 < -n < n_s$ , the holes populate the pair of bands at  $E \approx 0$ . In this scenario, the doping  $|n| = n_s/2$  is completely unremarkable, and

characterized by metallic transport. To create an insulating state instead of the metallic, we need to lift the remaining degeneracy between the bands to make sure that the Fermi energy lies within a gap between the split bands. Our mean field calculations show that this goal cannot be achieved with the order parameter (7) only [see Fig. 3 (a)], and an additional, inter-layer, order parameter is needed. To justify such an order parameter, our Hamiltonian, in addition to the Hubbard term (5), must have an inter-layer interaction:

$$H_{\text{int}}^{\perp} = \sum_{\mathbf{n}\mathbf{m}ss'\sigma} V(\mathbf{r}_{\mathbf{n}}^{1s} - \mathbf{r}_{\mathbf{m}}^{2s'}) \hat{d}_{\mathbf{n}1s\sigma}^{\dagger} \hat{d}_{\mathbf{n}1s\sigma} \hat{d}_{\mathbf{m}2s'\sigma}^{\dagger} \hat{d}_{\mathbf{m}2s'\sigma}, \quad (8)$$

which can be decoupled by the order parameter defined by

$$\Delta_{\mathbf{n}1s;\mathbf{m}2s'}^{\text{ex}} = V(\mathbf{r}_{\mathbf{n}}^{1s} - \mathbf{r}_{\mathbf{m}}^{2s'}) \langle \hat{d}_{\mathbf{n}1s\sigma}^{\dagger} \hat{d}_{\mathbf{m}2s'\sigma} \rangle. \quad (9)$$

For calculations we assume that  $\Delta_{\mathbf{n}1s;\mathbf{m}2s'}^{\text{ex}}$  is non-zero only for nearest-neighbor sites (for given  $\mathbf{n}$  and  $s$  in the first layer, the number of nearest neighbor sites in the second layer varies from 1 to 3, depending on  $\mathbf{n}$  and  $s$ ). As we have a new order parameter (9), the mean field Hamiltonian  $H_{\text{int}}^{\text{MF}}$  acquires additional terms associated with (9). Numerical calculations demonstrate that these terms induce qualitative modifications to the spectrum: all four low-energy bands become clearly separated from each other, see Fig. 2 (bottom). For this spectrum, the doping  $n = n_s/2$  is special: three lower flat bands are completely filled, while one upper band is perfectly empty. Similarly, at  $n = -n_s/2$ , one lower band is (completely) filled, all others are empty. Thus, the states at  $n \approx \pm n_s/2$  are insulating, in agreement with the experiment [25]. To estimate  $\sigma(n)$ , we use Eq. (4). This equation requires the knowledge of the functions  $\Delta_{\mathbf{m}i\sigma} = \Delta_{\mathbf{m}i\sigma}(n)$ , and  $\Delta^{\text{ex}} = \Delta^{\text{ex}}(n)$ . In principle,  $\Delta_{\mathbf{m}i\sigma}(n)$ ,  $\Delta^{\text{ex}}(n)$  can be determined self-consistently. Unfortunately, the required numerical self-consistency procedure is extremely laborious for the low- $\theta$  regime, and currently we cannot report any noticeable progress in this area. Luckily, important qualitative features of  $\Delta_{\mathbf{m}i\sigma}(n)$  and  $\Delta^{\text{ex}}(n)$  may be understood without such calculations. The reasoning is as follows. Near  $n = 0$  the order parameter  $\Delta_{\mathbf{m}i\sigma}$  opens a gap at the Fermi energy, pushing occupied bands to lower energy, reducing the total system energy. This implies that in the ground state  $\Delta_{\mathbf{m}i\sigma}(n = 0)$  is finite. On the other hand,  $\Delta^{\text{ex}}(n = 0)$  is small. Indeed,  $\Delta^{\text{ex}}$  lifts the degeneracy between two fully occupied bands; thus, the total energy of these bands is unaffected by non-zero  $\Delta^{\text{ex}}$ . At  $n \approx \pm n_s/2$  the roles of  $\Delta_{\mathbf{m}i\sigma}$  and  $\Delta^{\text{ex}}$  are reversed: the latter controls the splitting between occupied and empty bands, the former does not. Thus,  $\Delta^{\text{ex}}$  is finite at  $n = \pm n_s/2$ , while  $\Delta_{\mathbf{m}i\sigma}$  is suppressed. Keeping these trends in mind, we approximate  $\sigma(n)$  as follows: if  $|n| \approx 0$ , the conductivity is calculated for  $\Delta = 5.8 \times 10^{-3}t \cong 15$  meV [this value is

obtained self-consistently using Eq. (5)] and  $\Delta^{\text{ex}} = 0$ ; if  $n \approx \pm n_s/2$ , we use  $\Delta_{\text{mis}\sigma}(n = \pm n_s/2) = 0$  and  $\Delta^{\text{ex}}(n = \pm n_s/2) = 1.5 \times 10^{-3}t \cong 3.8 \text{ meV}$ . If  $|n| > n_s/2$ , both order parameters are assumed to be zero. For intermediate doping levels, we interpolate between these three regimes. The result is shown in Fig. 3 (c). It is consistent with the experiment [25]: the theoretical curve demonstrates pronounced dips both at  $n = 0$  and  $n = \pm n_s/2$ .

*Conclusions.*— Using a mean field approximation, we demonstrated that the four low-energy flat bands of TBLG at low- $\theta$  regime are very sensitive to interactions. Interactions lift the partial degeneracy between these four bands, inducing non-trivial many-body states. The degeneracy is lifted in two non-equivalent patterns: all bands may split apart, or two pairs of partially overlapping bands may emerge, depending on specific choices of the order parameters. We argue that, as the doping changes, a particular sequence of bands splittings is realized. This microscopic feature is manifested macroscopically as a doping-controlled sequence of metallic and insulating states. The resultant variation of conductivity is consistent with recent experimental observations [25].

This work is partially supported by the Army Research Office (ARO) under grant number 73315PH, the Russian Foundation for Basic Research (RFBR) and the Japan Society for the Promotion of Science (JSPS) under joint grant No. 17-52-50023. FN is supported in part by MURI Center for Dynamic Magneto-Optics via the Air Force Office of Scientific Research (AFOSR) (FA9550-14-1-0040), Asian Office of Aerospace Research and Development (AOARD) (Grant No. FA2386-18-1-4045), Japan Science and Technology Agency (JST) (the IMPACT program and CREST Grant No. JPMJCR1676), RIKEN-AIST Challenge Research Fund, and the John Templeton Foundation.

- 
- [1] A. Rozhkov, A. Sboychakov, A. Rakhmanov, and F. Nori, “Electronic properties of graphene-based bilayer systems,” *Phys. Rep.* **648**, 1 (2016).
- [2] M. Kharitonov, “Antiferromagnetic state in bilayer graphene,” *Phys. Rev. B* **86**, 195435 (2012).
- [3] R. S. Akzyanov, A. O. Sboychakov, A. V. Rozhkov, A. L. Rakhmanov, and F. Nori, “AA-stacked bilayer graphene in an applied electric field: Tunable antiferromagnetism and coexisting exciton order parameter,” *Phys. Rev. B* **90**, 155415 (2014).
- [4] D. S. de la Peña, M. M. Scherer, and C. Honerkamp, “Electronic instabilities of the AA-honeycomb bilayer,” *Ann. Phys. (Leipzig)* **526**, 366 (2014).
- [5] Y. Lemonik, I. Aleiner, and V. I. Fal’ko, “Competing nematic, antiferromagnetic, and spin-flux orders in the ground state of bilayer graphene,” *Phys. Rev. B* **85**, 245451 (2012).
- [6] J. Nilsson, A. H. Castro Neto, N. M. R. Peres, and F. Guinea, “Electron-electron interactions and the phase diagram of a graphene bilayer,” *Phys. Rev. B* **73**, 214418 (2006).
- [7] A. O. Sboychakov, A. L. Rakhmanov, A. V. Rozhkov, and F. Nori, “Metal-insulator transition and phase separation in doped AA-stacked graphene bilayer,” *Phys. Rev. B* **87**, 121401 (2013).
- [8] A. O. Sboychakov, A. V. Rozhkov, A. L. Rakhmanov, and F. Nori, “Antiferromagnetic states and phase separation in doped AA-stacked graphene bilayers,” *Phys. Rev. B* **88**, 045409 (2013).
- [9] T. C. Lang, Z. Y. Meng, M. M. Scherer, S. Uebelacker, F. F. Assaad, A. Muramatsu, C. Honerkamp, and S. Wessel, “Antiferromagnetism in the Hubbard Model on the Bernal-Stacked Honeycomb Bilayer,” *Phys. Rev. Lett.* **109**, 126402 (2012).
- [10] A. L. Rakhmanov, A. V. Rozhkov, A. O. Sboychakov, and F. Nori, “Instabilities of the AA-Stacked Graphene Bilayer,” *Phys. Rev. Lett.* **109**, 206801 (2012).
- [11] J. L. McChesney, A. Bostwick, T. Ohta, T. Seyller, K. Horn, J. González, and E. Rotenberg, “Extended van Hove Singularity and Superconducting Instability in Doped Graphene,” *Phys. Rev. Lett.* **104**, 136803 (2010).
- [12] M. Y. Kagan, V. A. Mitskan, and M. M. Korovushkin, “Phase diagram of the Kohn-Luttinger superconducting state for bilayer graphene,” *EPJB* **88**, 157 (2015).
- [13] M. Y. Kagan, V. V. Val’kov, V. A. Mitskan, and M. M. Korovushkin, “The Kohn-Luttinger effect and anomalous pairing in new superconducting systems and graphene,” *JETP* **118**, 995 (2014).
- [14] J. González, F. Guinea, and M. A. H. Vozmediano, “Electron-electron interactions in graphene sheets,” *Phys. Rev. B* **63**, 134421 (2001).
- [15] Y. E. Lozovik and A. Sokolik, “Electron-hole pair condensation in a graphene bilayer,” *JETP Lett.* **87**, 55 (2008).
- [16] Y. E. Lozovik and A. Sokolik, “Multi-band pairing of ultrarelativistic electrons and holes in graphene bilayer,” *Phys. Lett. A* **374**, 326 (2009).
- [17] A. O. Sboychakov, A. V. Rozhkov, A. L. Rakhmanov, and F. Nori, “Externally Controlled Magnetism and Band Gap in Twisted Bilayer Graphene,” *Phys. Rev. Lett.* **120**, 266402 (2018).
- [18] F. Zhang and A. H. MacDonald, “Distinguishing Spontaneous Quantum Hall States in Bilayer Graphene,” *Phys. Rev. Lett.* **108**, 186804 (2012).
- [19] F. Freitag, M. Weiss, R. Maurand, J. Trbovic, and C. Schönberger, “Spin symmetry of the bilayer graphene ground state,” *Phys. Rev. B* **87**, 161402 (2013).
- [20] P. Maher, C. R. Dean, A. F. Young, T. Taniguchi, K. Watanabe, K. L. Shepard, J. Hone, and P. Kim, “Evidence for a spin phase transition at charge neutrality in bilayer graphene,” *Nat. Phys.* **9**, 154 (2013).
- [21] W. Bao, J. Velasco, F. Zhang, L. Jing, B. Standley, D. Smirnov, M. Bockrath, A. H. MacDonald, and C. N. Lau, “Evidence for a spontaneous gapped state in ultraclean bilayer graphene,” *Proceedings of the National Academy of Sciences* **109**, 10802 (2012).
- [22] H. J. van Elferen, A. Veligura, E. V. Kurganova, U. Zeitler, J. C. Maan, N. Tombros, I. J. Vera-Marun, and B. J. van Wees, “Field-induced quantum Hall ferromagnetism in suspended bilayer graphene,” *Phys. Rev. B* **85**, 115408 (2012).
- [23] F. Freitag, J. Trbovic, M. Weiss, and C. Schönberger, “Spontaneously Gapped Ground State in Suspended Bi-

- layer Graphene,” *Phys. Rev. Lett.* **108**, 076602 (2012).
- [24] J. Velasco Jr., L. Jing, W. Bao, Y. Lee, P. Kratz, V. Aji, M. Bockrath, C. Lau, C. Varma, R. Stillwell, et al., “Transport spectroscopy of symmetry-broken insulating states in bilayer graphene,” *Nat. Nano* **7**, 156 (2012).
- [25] Y. Cao, V. Fatemi, A. Demir, S. Fang, S. L. Tomarken, J. Y. Luo, J. D. Sanchez-Yamagishi, K. Watanabe, T. Taniguchi, E. Kaxiras, et al., “Correlated insulator behaviour at half-filling in magic-angle graphene superlattices,” *Nature* **556**, 80 (2018).
- [26] Y. Cao, V. Fatemi, S. Fang, K. Watanabe, T. Taniguchi, E. Kaxiras, and P. Jarillo-Herrero, “Unconventional superconductivity in magic-angle graphene superlattices,” *Nature* **556**, 43 (2018).
- [27] J. M. B. Lopes dos Santos, N. M. R. Peres, and A. H. Castro Neto, “Graphene Bilayer with a Twist: Electronic Structure,” *Phys. Rev. Lett.* **99**, 256802 (2007).
- [28] R. Bistritzer and A. H. MacDonald, “Moiré bands in twisted double-layer graphene,” *PNAS* **108**, 12233 (2011).
- [29] G. Trambly de Laissardière, D. Mayou, and L. Magaud, “Numerical studies of confined states in rotated bilayers of graphene,” *Phys. Rev. B* **86**, 125413 (2012).
- [30] J. M. B. Lopes dos Santos, N. M. R. Peres, and A. H. Castro Neto, “Continuum model of the twisted graphene bilayer,” *Phys. Rev. B* **86**, 155449 (2012).
- [31] A. O. Sboychakov, A. L. Rakhmanov, A. V. Rozhkov, and F. Nori, “Electronic spectrum of twisted bilayer graphene,” *Phys. Rev. B* **92**, 075402 (2015).
- [32] E. J. Mele, “Interlayer coupling in rotationally faulted multilayer graphenes,” *J. Phys. D: Appl. Phys.* **45**, 154004 (2012).
- [33] A. Rozhkov, A. Sboychakov, A. Rakhmanov, and F. Nori, “Single-electron gap in the spectrum of twisted bilayer graphene,” *Phys. Rev. B* **95**, 045119 (2017).
- [34] S. Sorella and E. Tosatti, “Semi-Metal-Insulator Transition of the Hubbard Model in the Honeycomb Lattice,” *EPL (Europhysics Letters)* **19**, 699 (1992).
- [35] L. A. Gonzalez-Arraga, J. L. Lado, F. Guinea, and P. San-Jose, “Electrically Controllable Magnetism in Twisted Bilayer Graphene,” *Phys. Rev. Lett.* **119**, 107201 (2017).